Proceedings of the ASME 2025 44th International Conference on Ocean, Offshore and Arctic Engineering
OMAE2025
June 22-27, 2025, Vancouver, British Columbia, Canada

OMAE2025-156594

A VPP DERIVATIVE OPTIMISATION METHOD FOR WIND-ASSISTED CARGO SHIPS BASED ON RANSE-CFD

Lars Schmitz*
German Aerospace Center (DLR e.V.),
Institute of Maritime Energy Systems,
Geesthacht, Germany

Mark Leslie-Miller
Dykstra Naval Architects, Amsterdam,
Netherlands

Annika Fitz
German Aerospace Center (DLR e.V.),
Institute of Maritime Energy Systems,
Geesthacht, Germany

Sören Ehlers
German Aerospace Center (DLR e.V.),
Institute of Maritime Energy Systems,
Geesthacht, Germany

Marco Klein
German Aerospace Center (DLR e.V.),
Institute of Maritime Energy Systems,
Geesthacht, Germany

ABSTRACT

Wind Assisted Ship Propulsion (WASP) technologies represent a means to adhere to decarbonisation regulation, while ensuring an economic ship operation less dependent on future volatilities in fuel prices. As wind-assisted operation differs significantly from conventional operation with constant drift, heel and resultant induced resistance, there is significant potential in optimising hulls for sail-assistance.

The evaluation of the performance of a sail-assisted ship involves balancing all aerodynamic and hydrodynamic forces. Typically, a Velocity Prediction Program (VPP) is used for this task. For accurate predictions, a large amount of RANSE-CFD calculations is necessary, which makes performance evaluation and hull optimisation computationally costly.

In this paper, the VPP derivative method, is developed, which enables a far more efficient hull optimisation. The method focuses on specific operation conditions and employs RANSE-CFD simulations replicating these. To employ a VPP speed derivative selected key performance drivers are monitored. In this way, performance implications of hull variants may be evaluated in a very time efficient manner by a gradient approach.

Influence of the performance drivers is discussed and considerable performance increases are illustrated using a case study of a 130 m sail-assisted tanker vessel. Computational time per hull variation was cut down dramatically, while maintaining a satisfactory accuracy. The VPP derivative method proves to be a valuable tool to speed up the optimisation of a WASP ship hull.

Keywords: RANSE-CFD, WASP, VPP driven hull optimisation, gradient optimisation

*Corresponding author: lars.schmitz@dlr.de

NOMENCLATURE

β	Leeway angle [°]
CLP	Centre of lateral pressure [m]
F_x	Resistance in x [kN]
F_y	Side force [kN]
LCB	Longitudinal centre of buoyancy [m]
M_x	Righting moment [kN m]
M_z	Yawing moment [kN m]
T_p	Propeller thrust [kN]
TWA	True wind angle [°]
TWS	True wind speed [kts]
VCG	Vertical centre of gravity [m]
v_s	Ship speed [m/s]
v_x	Ship speed in x-direction [m/s]
v_y	Ship speed in y-direction [m/s]
WSA	Wetted surface area [m^2]

1. INTRODUCTION

WASP technologies have attracted increased interest in recent years as a means to reduce the carbon footprint while ensuring economic ship operation. The global push for decarbonisation and expected volatility in fuel prices have sparked a renewed regard to harness wind power to complement conventional propulsion. WASP technologies enable ships to reduce fuel consumption and emissions, thus providing a means to adhere to decarbonisation regulation [1–3]. With positive effects as conformity with decarbonisation regulation, decreased operational risk due to volatility in fuel (and future fuel) prices and a positive impact on a companies public perception [4–7], there is a considerable uptake of the technology. Studies, as well as classification societies reports, observe an increase in installations and expect a massive boost of installations in the coming years [7–13]. With

uptake of the technology originating from a broader range of ship types and increased trust in the technology, some see WASP technologies "on the verge of a tipping point" [10].

A vast amount of installed WASP systems to date are retrofits [10], however, the highest potential for fuel saving is expected for ship hulls optimised for wind-assistance [14–16]. Incorporating additional structure, needed for large sail systems, is more costly and difficult while retrofitting. When addressing these issues at an early design stage, larger sails and thus higher potential savings may be generated [9]. Another important factor for large energy savings through WASP deployment is the optimisation of the ship hull for sail-assistance to achieve a balanced design and low side force induced resistance [14, 17, 18].

Literature on hull optimisation for WASP vessels is scarce, also due to the huge computational effort necessary. Recent studies focused on improving specific performance drivers as side force production and side force induced resistance or the longitudinal position of the centre of lateral pressure (CLP) as a measure for the yaw balance [16, 17, 19]. However, it is recognised that an integrated optimisation approach is essential. This entails the use of CFD [19] as well as of a VPP or Power Prediction Program (PPP) [20]. Furthermore, it is concluded, that the relation between side force production and side force induced resistance is too complex to be evaluated using simplified models [16], making it imperative to apply high fidelity and holistic models for these aspects. Therefore, to judge the influence of a hull parameter or alteration on sail ship performance, the use of a VPP is imperative to account for the side force induced resistance and other effects due to the sail equilibrium [16, 21]. Using the VPP and high fidelity methods as input allows optimisation for realistic conditions with high accuracy, but entails a range of CFD simulations and thus high computational effort.

In this paper, a time efficient optimisation method, the VPP derivative method, for sailing vessels and WASP vessels is introduced. The method addresses the above mentioned issues by providing significant time savings, while taking into account the sailing balance and high fidelity evaluation of the physics involved. This is achieved by employing a VPP driven gradient method and evaluating the key performance drivers using high-fidelity methods as RANSE-CFD.

2. METHODOLOGY

The methodology has been split into three parts. A description of selected physical phenomena exceptionally important for sailing or sail-assisted vessels and resultant performance drivers in Sec. 2.1. A sum up of the methods used to evaluate performance, amongst others through the VPP and the CFD simulations performed as input to the VPP in Sec. 2.2. And the third part, Sec. 2.3, describes the VPP derivative optimisation method. A flow chart, which visualizes the steps undertaken in the optimisation process for the base vessel and each hull variant as conducted for the case study, see 3.1, is presented in Fig. 1.

2.1 Physical Phenomena and Performance drivers

The physics of sailing are characterized by complex interactions of different systems and forces. The sail ship will often operate in equilibrium conditions with a constant non-zero leeway β, heel and rudder angle. These, by far, exceed the range of simplification due to small angles, often introduced in conventional ship design. In these equilibrium conditions, different physical phenomena, than prevailing in conventional ships, come to play and have non-negligible effects on ship resistance and efficiencies.

The aerodynamic side force must be effectively balanced by corresponding hydrodynamic reaction forces to limit drift and utilize the produced thrust. Thus, side forces exerted by the hull and its lifting surfaces become relevant for WASP vessels. Side force production can be separated into two main principles, cf. [13].

- Circulatory lift, analogous to the lift created by an infinite airfoil. This dominates on rudders and high aspect-ratio appendages as dagger boards or fins.

- Cross-flow drag, describing momentum transfer from the ship to vortices separating in the flow. Cross-flow drag occurs at the tip of a rudder, around bilge radii or bilge keels.

Associated with the side force exerted by the hull, there is a leeway or side force induced resistance, which often may be larger than the hull's resistance [17, 22]. High amounts of side force induced resistance are caused particularly by cross-flow drag [13]. A metric to model side force induced resistance and thus sailing efficiency is the effective draught defined in analogy to [23].

The aerodynamic side force causes the ship to move with a constant leeway angle. The munk moment, cf. [24], acting on all slender bodies in oblique flow causes a large yawing moment. On unbalanced ships with unsuitable centre of lateral pressure (CLP), the occurring yaw moment must be balanced by high static rudder angles, causing additional resistance. Alternatively, the sail area and drive force must be reduced prematurely [25–27], which is often the case on retrofitted ships.

The heeling moment caused by the WASP systems may also lead to added resistance through altered wetted surface area (WSA) and pressure distribution around the hull [13]. Additionally, the propeller will operate in lightly loaded condition due to the drive force of the WASP systems and in oblique flow due to the leeway. Loading and oblique flow impact thrust, engine and propeller efficiency, which may decrease, but also increase efficiency [12, 28, 29].

These considerations lead to four performance drivers for the hydrodynamic performance of a WASP ship, see also [16, 19].

- Hull resistance in x- direction, which includes aspects of side force induced resistance and heel induced resistance

- Side force production

- Stability/Righting moment

- Yaw balance, represented by the longitudinal centre of lateral pressure (CLP)

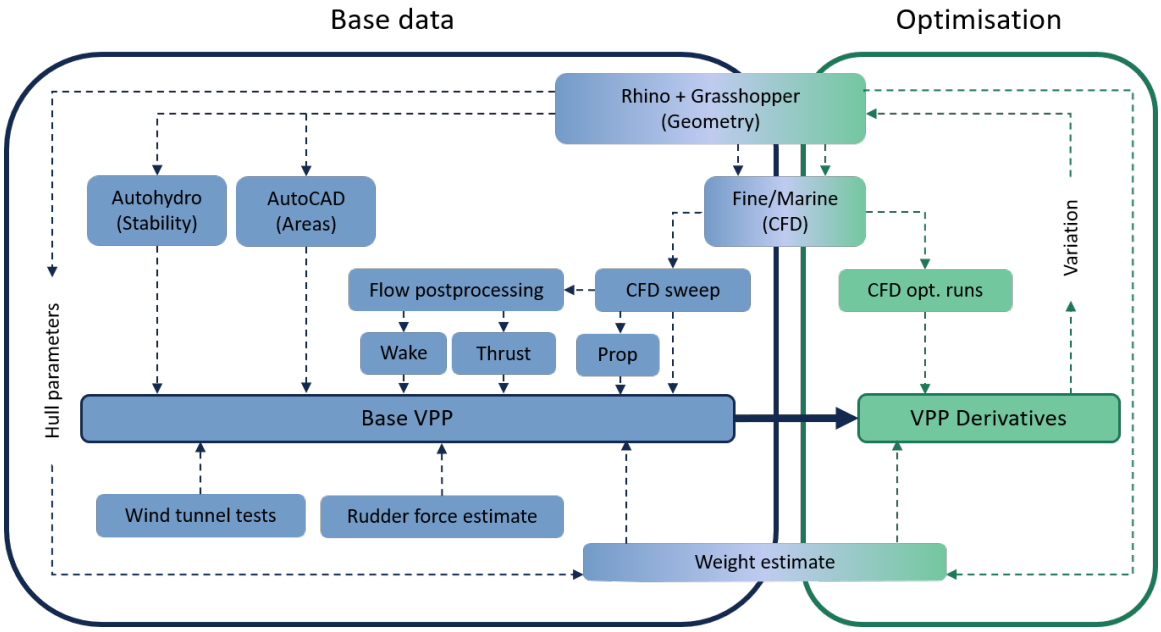

FIGURE 1: PROCESS OVERVIEW. FLOW CHART OF STEPS UNDERTAKEN IN OPTIMISATION PROCESS FOR BASE VESSEL AND EACH HULL VARIANT.

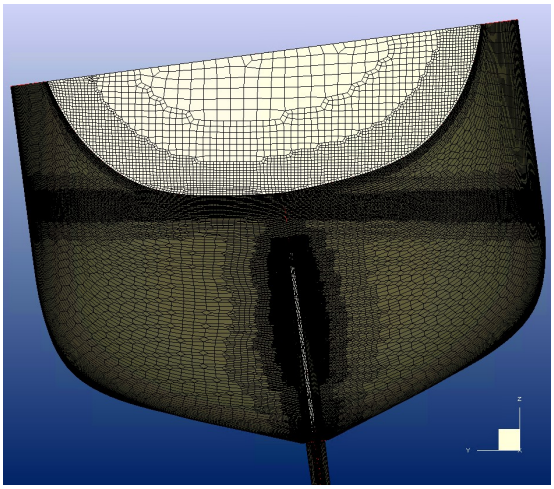

FIGURE 2: MESH VISUALISATION FOR CASE STUDY IN FULL SCALE WITH A LENGTH OF 130 M AND A BEAM OF 18.9 M.

2.2 Performance Evaluation

Following the industry standard as described in [30], a steady-state 6-Degrees of Freedom (DoF) VPP is used to evaluate performance of the ship. A VPP finds equilibrium conditions between all occurring aerodynamic and hydrodynamic forces and moments by solving the following equation system, cf. [31].

$$\begin{cases} 0 = \sum \overline{F_x} = \overline{F_{H,x}} + \overline{F_{A.x}} \\ 0 = \sum \overline{F_y} = \overline{F_{H,y}} + \overline{F_{A.y}} \\ 0 = \sum \overline{F_z} = \overline{F_{H,z}} + \overline{F_{A.z}} + \overline{W} + \overline{\Delta} \\ 0 = \sum \overline{M_x} = \overline{M_{H,x}} + \overline{M_{A.x}} + \overline{M_{R,x}} \\ 0 = \sum \overline{M_y} = \overline{M_{H,y}} + \overline{M_{A.y}} + \overline{M_{R,y}} \\ 0 = \sum \overline{M_z} = \overline{M_{H,z}} + \overline{M_{A.z}} \end{cases} \quad (1)$$

Here, subscript A and H indicate forces (F) and moments (M) stemming from the aerodynamics (A) and their direct hydrodynamic (H) counterparts. $\overline{W}$ refers to the ship's weight and $\overline{\Delta}$ to the resultant displacement. Pitching and heeling moments induced by aerodynamic forces are balanced by hydrostatic righting moments $\overline{M_R}$. Forces and Moments are defined in the ship coordinate system. Separating aerodynamic and hydrodynamic forces and using averaged forces in a steady-state approach, as outlined in [32], introduces a simplification of the physics. However, these simplifications represent the industry state-of-the-art [30, 32–35] and show a "feasible balance of accuracy and computational cost for an industrial purpose" [30]. For the scope of this paper, the in-house VPP of Dykstra Naval Architects (DNA) was used, see [35]. The VPP accounts amongst others for multiple lifting surfaces, rudder, incorporates a propeller model including added drag, motor-sailing conditions and propeller-hull interactions as well as aerodynamic parasitic drag from hull and superstructure. Using physical, high fidelity input data by means of wind tunnel tests for the sails and RANSE-CFD, the VPP has been validated in real-life conditions [31].

The ITTC Guidelines [30] define the modelling basis for a level suitable for a business case and reliable performance prediction. It requires aerodynamic modelling through validated CFD or wind tunnel tests, as used in the case study introduced herein, cf. 3.1. Hydrodynamic modelling of hull and appendages requires model tests or CFD simulations.

Here, RANSE-CFD simulations were conducted in the commercial software Numeca Fine/Marine. In accordance with the CFD Softwares Best Practices, the simulations were set up as unsteady pseudo-transient simulations, to ease convergence of the free surface. The simulations were conducted with two DoF, sinkage and trim, for a range of speeds, leeway angles and heel angles. The Volume of Fluid (VOF) method was applied to resolve

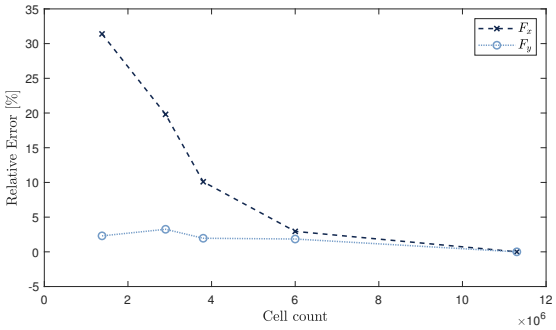

FIGURE 3: CONVERGENCE STUDY F_x AND F_y. HEELED 10 ° AND WITH 6 ° OF LEEWAY. DISPLAYED IS THE RELATIVE ERROR IN % IN RELATION TO THE FINEST MESH EXAMINED.

the free surface and the turbulence model $k-\omega\,SST$ was used. The third-order AVLSMART scheme was employed for spatial discretisation. For temporal discretisation, an implicit multi-step approach, in FineMarine referred to as sub-cycling acceleration, was used with a variable time step, depending on ship speed. The mesh was set up according to correlation with towing tank results for similar ship designs and also according to a spatial convergence study. The study was conducted for two different operational conditions, including heel and leeway. Five different meshes with varying cell count were studied. Results for one operational conditions and forces in x and y are presented in Fig. 3. The chosen mesh features a cell count of $\approx 5.9 \times 10^6$ cells and ensures relative errors in comparison to the converged solution below 3 % here. Refinements were applied on the free surface and in relevant locations on the hull, as the bow, appendages and appendage tips. The boundary layer has been resolved with a maximum $y+$ value of 300 and a wall function has been applied. A snapshot of the mesh is shown in Fig. 2. To study propeller-hull interactions, self-propulsion and behaviour in oblique flow, an actuator disc model was applied to selected cases. For the exact hull shape of the case study, there have not been any towing tank tests conducted. However, for a range of parent hull shapes, there have been extensive towing tank tests and CFD simulations conducted to validate the CFD simulation setup in [36, 37]. The here conducted simulations have been set up in accordance with [36, 37] as well as following the proven simulation setup from Dykstra Naval Architects.

2.3 VPP derivative optimisation

The main aim of the work conducted for this paper is the development of an efficient optimisation method to improve ship hulls for sailing operation. The objective function could be power savings on a given route or in specific conditions. Alternatively, the speed of a wind-assisted ship in specific conditions at constant thrust or power input could be maximised. The latter is also applicable for ships solely propelled by the sail systems and may be evaluated more directly. For these two reasons, ship speed was chosen as objective function, for this case study. The method is equally applicable for power savings as objective function. Case study specific constraints are imposed in form of geometry, displacement and class rules (e.g., stability).

Sail ship performance in specific conditions is highly dependent on the delicate sail equilibrium between aerodynamic and hydrodynamic forces, as outlined above in Sec. 2.2. Small changes of hull geometry may lead to large differences due to yaw balance, heel and side force induced resistance. Thus, to judge the influence of a hull parameter or alteration on performance, the use of a VPP is imperative to capture effects caused by a different sail equilibrium, see [21]. However, a large number of CFD simulations are necessary to ensure reliable results when analysing a ship hull through a VPP. If a new VPP has to be tuned for every hull variant, with a large number of implied CFD simulations, optimisation is computationally very costly. A parametric optimisation study would entail a very large number of evaluated designs, depending on number of parameters [21], which amplifies the aforementioned aspect. A VPP driven gradient optimisation, as the here proposed VPP derivative optimisation, "is deemed significantly more efficient" [21]. In the gradient optimisation method, input parameters are slightly perturbed to approximate

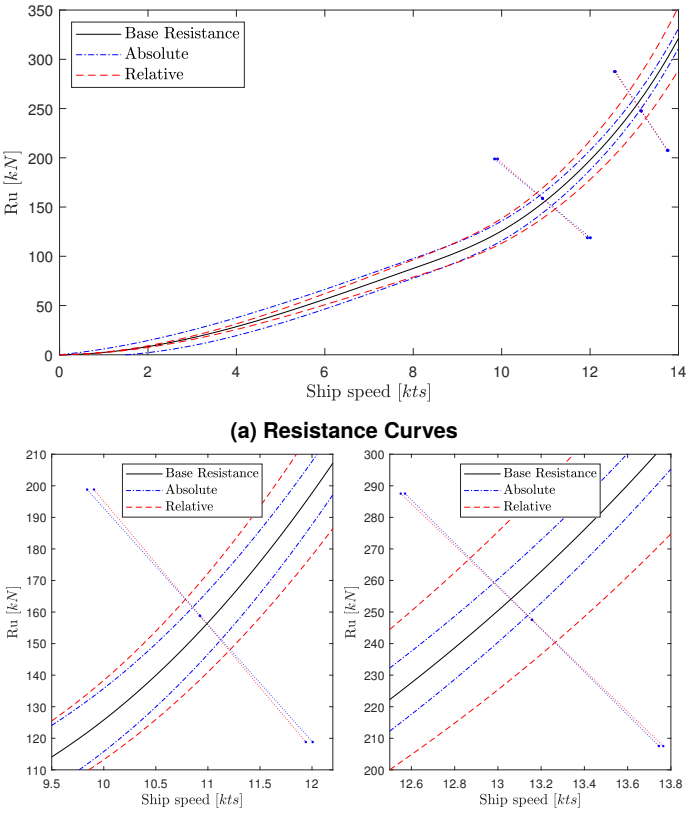

(a) Resistance Curves

(b) Detail - Operation Point 1 **(c) Detail - Operation Point 2**

FIGURE 4: ABSOLUTE AND RELATIVE VPP DERIVATIVE METHOD IN COMPARISON. CONTINUOUS LINE REPRESENTING THE BASE RESISTANCE CURVE, BLUE DOT-DASHED LINE REPRESENTING THE ABSOLUTE APPLICATION AND THE RED DASHED LINE REPRESENTING THE RELATIVE APPLICATION. IN DETAIL, THE INFLUENCE ON PREDICTED SPEED BY A RESISTANCE INCREASE AND DECREASE BY 40 KN AT TWO OPERATION POINTS ARE SHOWN. THE DOTTED LINES REPRESENTS THE SLOPES AT THESE POINTS AND THE HORIZONTAL DISTANCE BETWEEN THE DOTTED LINES EQUALS THE DIFFERENCE IN PROGNOSED LOSS IN VELOCITY DUE TO THE RELATIVE OR ABSOLUTE APPLICATION METHOD.

its effect on the objective function for example via the finite difference method. Thus, a suitable path to further optimisation can be found [21]. In the VPP derivative method, the gradient approach is applied twice, as described below, to solve both the aforementioned problems. The first application of the gradient approach, through the VPP derivative method, eliminates the need to recalculate the full VPP for each hull variant, thus saving considerable time. The second application of the gradient approach serves as an outer optimisation process and could theoretically be replaced by alternative methods of multi parameter optimisation.

It is imperative to use a reasonable design as baseline, as otherwise the method will become inaccurate with changes too large or even become unstable. Exactly how large changes are allowed to be will need to clarified in further research. However, the baseline design should not be purposely unbalanced just to achieve large improvements, otherwise the scope and applicability of the method may quickly be overstepped. Additionally, key parameters and dimensions should roughly align with the expected final design. As an example, variation in total displacement or stability may cause large changes not covered by the method. If those occur, it might be necessary to re-initiate the method by establishing a new baseline.

To enable use of the method, operational conditions to be optimised for need to be chosen, here shortened to operation points. They should consist of representative true wind speeds (TWS) and true wind angles (TWA), based on prevailing wind conditions or encountered conditions en route to optimise for the operation profile. Using a VPP for the base design, the equilibrium conditions may be calculated for these operation points. Outputs will be amongst others ship speed v_s, resistance F_x, propeller thrust T_p, side force F_y, resulting leeway angle β, heel/righting moment M_x and resulting heel angle. Based on the operation points and the resulting equilibrium forces, specific CFD simulations are set up. To minimize computational effort, they may be clustered together for example to minimize meshing or initiation simulations. Care should be taken to not distort the operation points overly. Direct output of the simulations should be the performance drivers selected for the optimisation. The four performance drivers, presented in Sec. 2.1, are evaluated through the VPP derivative optimisation. However, the method would also work for different performance drivers, as long as these are output of a CFD simulation. This could be relevant for ship designs which are sensitive to specific physical phenomena. In this case study, the evaluated performance drivers are:

- Hull resistance F_x
- Side force F_y production, evaluated as leeway angle β through the relation between v_x and v_y for an imposed (aerodynamic) side force F_y
- Righting moment M_x, which needs to be superimposed with changes in hydrostatic righting moment due to change in VCG
- Yaw balance, evaluated through the CLP position by $CLP = M_z/F_y$, when correcting for the origin.

For each of the performance drivers, the impact on the objective function or here ship speed is straight forward to conclude. The VPP derivative method aims at weighing the trade-offs between these without having to conduct all the simulations necessary for a full VPP. Assuming linear behaviour for the effect of small geometry variations, the theoretical effect of an isolated change in one of these performance drivers can be estimated by rerunning the VPP, but with slightly perturbed values for each single performance driver. Using the applied perturbations of the performance drivers and the resultant ship speeds as output from the VPP at the operation points, finite differences or derivatives can be formed in the following shape:

- $\frac{\mathrm{d}v_s}{\mathrm{d}F_x}$ - Speed delta due to difference in upright resistance,
- $\frac{\mathrm{d}v_s}{\mathrm{d}\beta}$ - Speed delta due to difference in leeway angle β at constant side force,
- $\frac{\mathrm{d}v_s}{\mathrm{d}M_x}$ - Speed delta due to difference in righting moment at constant heel angle,
- $\frac{\mathrm{d}v_s}{\mathrm{d}CLP}$ - Speed delta due to difference in centre of lateral pressure CLP.

When running a CFD simulation, which reflects an operation point with index i, the output of the performance drivers can be converted to a speed delta caused by the change of hull geometry. The overall impact of a geometry variation for a specific operation point is the sum of speed deltas:

$$dv_{s,i} = \frac{\mathrm{d}v_s}{\mathrm{d}F_x}\cdot dF_{x,i} + \frac{\mathrm{d}v_s}{\mathrm{d}\beta}\cdot d\beta_i + \frac{\mathrm{d}v_s}{\mathrm{d}M_x}\cdot dM_{x,i} + \frac{\mathrm{d}v_s}{\mathrm{d}CLP}\cdot dCLP_i. \quad (2)$$

Overall performance improvement of the ship may be judged by choosing weight factors w_i for each operation point based for example on occurrence along the route.

$$dv_{s,tot} = \sum_{i=1}^{n} w_i \cdot dv_{s,i}. \quad (3)$$

And here, the gradient method can be applied a second time with regards to the change of parameter in hull optimisation. This streamlines optimisation in analogy to [21]. Direct accounting of motor-sailing operation is possible either through the VPP or for example by incorporating an actuator disc into the simulations.

The perturbations to the performance drivers can generally be introduced by two different methods. Either by applying a relative change or an absolute offset. By applying a relative change, the curves, e.g. the resistance curve, is distorted, however, the physical behaviour may be replicated more accurately. By applying an absolute offset, the character of the curve is not changed. In case of the resistance curve this leads to a high difference in speeds due to the perturbation if the operation points feature very different base speeds. Also, this may invite extrapolation or low accuracy due to a too large perturbation in some cases. The behaviour for the different application methods is presented for the resistance example in Fig. 4. Questionably, it will depend on the physical behaviour of the performance driver, which method should be favored. Both application approaches were investigated for this study.

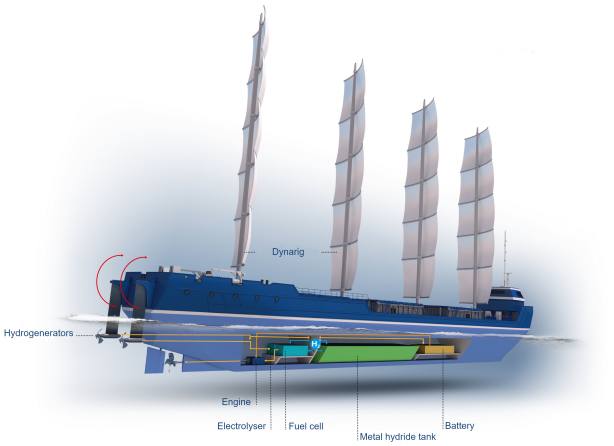

FIGURE 5: VISUALIZATION OF PROPULSION CONCEPT OF THE CASE STUDY BY DLR

By applying the VPP derivative optimisation method, as outlined above, a VPP driven optimisation is enabled, thus accounting for effects of the sail equilibrium. Meanwhile, only one CFD simulation per operation point needs to be conducted, instead of a large sweep of CFD simulations, which would be needed to recalculate the VPP for each hull variant, without the VPP derivative method.

3. RESULTS AND DISCUSSION

Following, the case study is briefly introduced and some of the results achieved through the use of the VPP derivative optimisation method are shown in Sec. 3.1. Then, the VPP derivative method is evaluated and the two application methods are discussed in Sec. 3.2.

3.1 Case Study

This paper aims at describing the optimisation method itself. For this reason, overall performance impact and conclusions are shown here for the case study. However, detailed description, individual hull variations and optimisation results of the case study extend beyond the scope of this paper.

The investigated case study is a 130 m sail-assisted tanker vessel, which is based on the Ecoliner concept by Dykstra Naval Architects, cf. [38] as well as prior optimisation work [39]. Furthermore, the study was incorporated into a feasibility study within the German Aero Space Centre (Deutsches Luft- und Raumfahrtzentrum) (DLR) for a carbon neutral tanker with a liquid hydrogen propulsion train, see Fig. 5. Constraints, boundary conditions and potential routes were imposed by the goals of the study. The focus here was solely on hull and appendage optimisation. Thus, the rig and sail systems were out of scope and were adopted from a similar project, where wind tunnel test data could be made available for the complete Dynarig system with four masts.

Geometry creation, variation and parametric modification took place in Rhino®, as well as Grasshopper®. An appropriate weight estimation in the concept phase is key to establish the feasible deadweight necessary for techno-economic analysis but also to estimate the vertical centre of gravity (VCG) and thus stability. The VCG is a vital input to the VPP for realistic sailing performance, but also to fulfil safety regulation. Ship hull weight was approximated empirically based on [38, 39] by following procedure and formulae contained in [40, 41]. Weight of the rig system, tank system and the retractable centreboard were added based on manufacturer information or estimations. The VCG was updated and superposed for each new hull design.

To create a reasonable baseline design as mentioned in Sec. 2.3 and follow the case study constraints, the Ecoliner was scaled and reshaped accordingly. The case study aimed at showing maximum savings in wind-assisted mode and carbon neutral operation. Thus, a simple skeg and a retractable high aspect-ratio centreboard were added to the base design to boost sailing performance.

The ships performance was optimised for operation on two routes and corresponding wind conditions:

- Hamburg (Germany) ↔ Walvis Bay (Namibia)
- Hamburg (Germany) ↔ Valparaiso (Chile) via the Panama Canal

Constraints were set amongst others by the depth of the harbours at a minimum of 13.8 m, as well as by the height of the bridges across the Panama Canal at 62.5 m. There was no weather routing conducted for this case study. The prevailing wind conditions en route originated from statistical weather data on assumed routes gathered through the 'Blueroute' tool by MARIN [42]. These wind conditions were condensed to five operation points as shown in Table 1, adding motor assistance when sailing speeds were insufficient. These contain a pure motoring case at 10 kts to monitor the detrimental impact of the optimisation for sailing on the motoring operation. Operation points two and three are motor-sailing cases which include an actuator disc in the CFD simulation and thus also account for oblique flow on the propeller. Operation points four and five are pure sailing cases. Extrapolating prevailing wind conditions from an initial weather routing could be a sensible approach for justifying operation points in further research.

A large number of hull variations were tested during the optimisation process. These variations included pure hull form variation as bilge radius, LCB position or transom immersion,

TABLE 1: CONDENSED CONDITIONS FOR THE FIVE OPERATION POINTS TO BE USED AS INPUT FOR CFD

	Operation points				
	1	2	3	4	5
TWS [kts]	0	12	10	14	18
TWA [°]	0	155	70	70	105
v_s [kts]	10.0	7.0	9.5	11.0	13.0
AD [kW]	-	200	200	-	-
T_{AD} [kN]	-	34.6	15.2	-	-
Q_{AD} [kNm]	-	24	14	-	-
heel [°]	0	0	7.5	7.5	7.5
SF [kN]	0	11	200	330	250

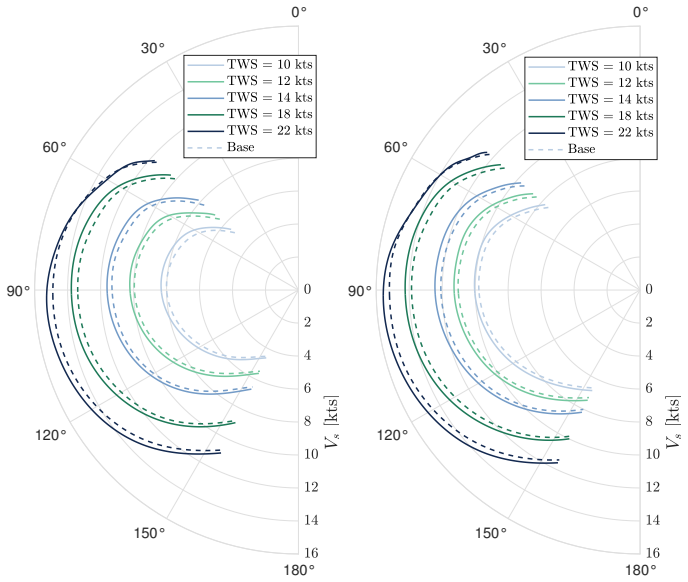

(a) Pure sailing **(b) Motor-sailing**

FIGURE 6: POLAR DIAGRAM OF PERFORMANCE OF OPTIMISED VS. THE BASE DESIGN. ACHIEVED SHIP SPEEDS FOR A VARIETY OF TRUE WIND SPEEDS (TWS) OVER TRUE WIND ANGLES (TWA). SOLID LINE REPRESENTS THE OPTIMISED GEOMETRY, DASHED LINE REPRESENTS THE BASE DESIGN. IN MOTOR-SAILING CONDITION, A CONSTANT SHAFT POWER OF 200 KW IS APPLIED.

but also appendage variations regarding, for example, the skeg shape or centreboard shape and position. At constant wind conditions and engine power, considerable speed increases of more than 2.8 % on average were recorded. For the motoring case at 10 kts, the shaft power was decreased by more than 4 %. The performance difference between the base design and the current optimised design for the pure sailing and motor-sailing case are illustrated in Fig. 6 in the form of a polar diagram.

The high aspect-ratio appendages as centreboard and the skeg perform very efficiently. The majority of side force production can be accounted to these two and the rudder. Depending on the conditions, roughly 40 % of the hulls side force, excluding the rudder, is produced only by the retractable centreboard, see also Fig. 7. This minimizes drift and side force induced resistance, which can account for large parts of a sailing ships resistance, cf. [17]. Large improvements of performance were also due to the skeg design. A profiled skeg with a pronounced leading edge, stimulated circulatory lift production without any drawbacks. This behaviour is reflected by an increase of effective draught, see 2.1, by 1.3 m or around 10 % at 3° of leeway angle and 14 kts speed.

3.2 Evaluation of VPP derivative method

The main aim of this paper is to introduce the VPP derivative method and to discuss two different application methods of perturbation of the performance drivers as explained in Sec. 2.3.

The two application methods may be generalized as applying perturbations as an absolute offset (DV1) or by applying a relative change (DV2). It was assumed that the accuracy of the application approach depends on the physical behaviour, that is aimed to

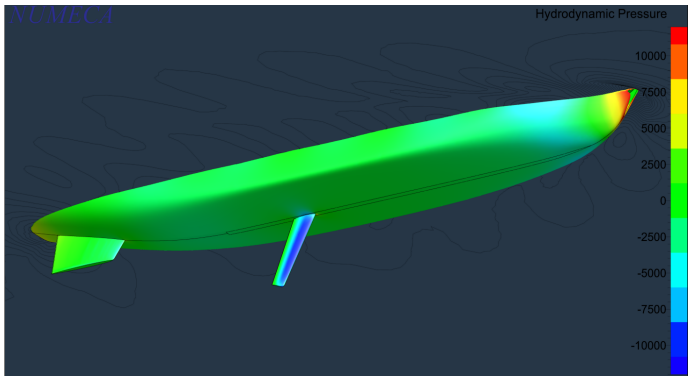

FIGURE 7: DYNAMIC PRESSURE DISTRIBUTION ON HULL AND APPENDAGES AT OPERATION POINT 4.

be replicated. Following this assumption, the righting moment derivative would best be approached by an absolute method by mimicking a change in metacentric height (GM). As yaw balance mostly influences ship speed through induced resistance from the rudder, as well as through sail trim, its behaviour should also best be estimated by a relative perturbation. A relative increase should replicate a resistance increase best, as ship resistance is approximately proportional to the square of the speed. However, side force induced resistance is included in the resistance derivative and not in the side force derivative, thus, there is a link between the two. Furthermore, it depends on the mode of side force production as to which application method might be most suitable. There are linear as well as non-linear side force components. An example for non-linearity is side force production through separation, see [13], while circulatory lift before separation is an example for linearity [43]. Since the composition of side force production is unclear, so is it unclear which methods should be favoured for the side force derivative.

Generally, it must be noted, that only the overall accuracy of the methods may be judged and a combination of the two application methods may well be favourable. The validation data for the derivative methods consists of the VPP results of the initial base line design of the case study and of those of the final optimised design and thus of overall speeds or speed differences. It is not possible to account parts of the speed difference to a specific derivative with these. In Table 2, the achieved speed differences at the operation points, calculated through the VPP, are compared to the prognosis of speed differences through the VPP derivative method. Also, the relative errors are displayed. The relative error is here defined as the percentage wise difference between the speed increase as forecasted by the VPP derivative method and the resultant speed increase calculated through the full VPP. The speed differences in comparison and also the composition due to the derivatives components is displayed in Fig. 8. At Points 2, 3 and 4, the derivative methods underestimate the achieved speeds, at Point 5, the derivative methods overestimate the achieved speed.

Especially at Points 2 and 3 the errors according to the VPP derivative methods are large. With the absolute method the error amounts to almost 70 % and 35 % respectively, with the relative method almost to 45 % and 11 %. At Points 4 and 5, so the

TABLE 2: ACHIEVED SPEEDS IN COMPARISON BETWEEN THE FINAL OPTIMISED DESIGN AND THE BASE DESIGN WITH RESULTS FROM THE VPP AND THE VPP DERIVATIVE METHODS ALONG WITH THE EXPERIENCED ERRORS. THE AVERAGE VALUE GIVEN, IS THE AVERAGE OF THE ABSOLUTE VALUE.

	VPP CALC			DERIVATIVES			
Point	$dv_{s,base}$ [kts]	$dv_{s,final}$ [kts]	dv_s [kts]	$dv_{s,DV1}$ [kts]	$dv_{s,DV2}$ [kts]	$Error_{DV1}$ [%]	$Error_{DV2}$ [%]
2	7.19	7.37	**0.18**	**0.05**	**0.10**	-69.4	-43.9
3	9.56	9.85	**0.29**	**0.19**	**0.26**	-35.1	-10.9
4	10.92	11.25	**0.33**	**0.30**	**0.28**	-7.0	-12.6
5	13.16	13.53	**0.37**	**0.39**	**0.41**	5.2	11.2
Average:			0.29	0.23	0.26	29.2	19.6

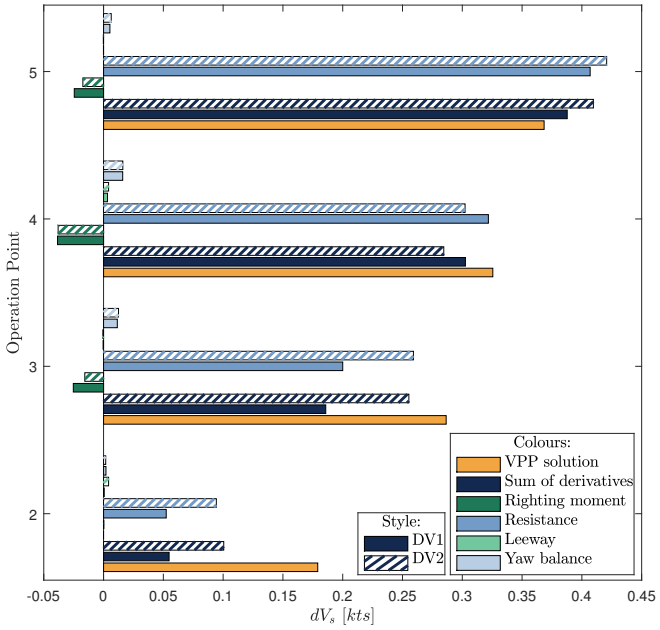

FIGURE 8: VPP DERIVATIVE EVALUATION: COMPOSITION AND COMPARISON. COMPOSITION OF SPEED DIFFERENCE DUE TO DERIVATIVE COMPONENTS IS SHOWN IN COMPARISON FOR THE TWO DERIVATIVE METHODS (ABSOLUTE METHOD (DV1) FILLED AND RELATIVE METHOD (DV2) HATCHED) AND IN COMPARISON TO THE OVERALL SPEED DIFFERENCE RESULTING FROM THE FULL VPP

pure sailing cases, however, the errors are relatively small, with a maximum error of 12.6 %. The operation points, experiencing large errors, are motor-sailing points using an actuator disc. The errors between point 2 and 3 scale approximately with the produced thrust, refer to Table 1. Thus it may be concluded there has been an error with accounting for the actuator disc in the VPP derivative method.

Nonetheless, with the substantial geometry variations implemented, the prediction of the derivative methods shows a satisfactory accuracy. For the two pure sailing conditions, the absolute derivative method (DV1) exhibits an average error of 6.1 % and the relative derivative method (DV2) of 11.9 %. Both are in an acceptable range for the purpose. It is interesting, that here, the absolute derivative showcases a higher accuracy than the relative derivative, even though, over all conditions, the relative derivative features a higher accuracy. From Fig. 8 it becomes obvious, that the predicted speed differences are very much resistance derivative driven. This is due to pure resistance, but also because side force induced resistance is also included, which both are major drivers for WASP sailing performance. However, since it was expected, that the resistance derivative is better applied in a relative way, the superior performance of the absolute method at the sailing operation points comes as an even bigger surprise. The here featured leeway angles β are small, and a majority of the side force is produced by high-aspect ratio lifting surfaces as centreboard, rudder and skeg and thus through circulatory lift. Due to the small angles of attack, they can be presumed to operate in the linear area of the lift and drag curves, cf. [43]. Arguably, the behaviour of the side force induced resistance at these angles of attack is best mimicked by an absolute offset, which could be an explanation for the good performance of the absolute derivative. This should be investigated in further research.

A potential source of errors is extrapolation past the linearisable amount of changes. By rerunning the VPP derivative calculation for the final model, the new slopes of each derivative and operation point may be calculated. If they substantially deviate from the original slopes, this poses a source of error. In general, the final slopes of the derivatives were very close to the original slopes. However, the righting moment derivatives deviated more than the others, by up to 28 % at Point 5. This might have skewed the results and accuracy of the VPP derivative method as employed here.

The errors of the VPP derivative method shown in Table 2, especially in the pure sailing cases, are in an acceptable range. But they are much larger than the nuances of speed differences between single hull variations tested in the case study. Thus, when only small differences in speed are predicted by the VPP derivative method, the applicability of the method is a question of if the trends are depicted correctly, even though the absolute value might be over- or underestimated.

Overall, the method enables VPP driven hull optimisation in a computationally efficient manner. As described in Sec. 2.3, a much smaller number of CFD simulations may be conducted per hull variant by employing the VPP derivative method in comparison to recalculating a VPP for each hull variant, while still using a VPP driven optimisation and incorporating effects caused by

the sail equilibrium. For the five operation points analysed for the case study, a total of nine CFD simulations were run per hull variant, including initialization simulations to maximise overall speed. To calculate a full VPP for a hull variant, here, a total of 21 simulations were necessary. Overall computational effort per hull variation was cut down by two thirds, through reduced number of simulations, meshing time and by not recalculating the VPP.

4. CONCLUSION AND OUTLOOK

In this paper, a VPP driven gradient optimisation method named the VPP derivative method has been developed. Different perturbation approaches of the VPP derivative method, namely an absolute and a relative change, were applied and compared. Using the case study of a highly performant 130 m sail-assisted tanker vessel, originally based on the Ecoliner by Dykstra Naval architects, the applicability of the method was shown, especially when judging the impact of efficient high aspect-ratio appendages.

The VPP derivative method proves to be a valuable tool in weighing the effect on speed of different phenomenons and variations against each other. Total speed difference was predicted in an acceptable range. Over all operation points, the relative derivative method performed a bit better than the absolute derivative method. However, it is suspected, there was a flaw in the method of implementing the actuator discs into the VPP derivative method, which should be investigated in further research. In the pure sailing cases, the absolute derivative method outperformed the relative derivative method. Both application methods showed a reasonable accuracy. The comparison of the two application methods in total was inconclusive and requires more attention.

Further research should be conducted to evaluate which application method should be favoured as well as suitable performance drivers. This could consist of tests with additional application methods or a combination of absolute and relative application. The effect of side force production on the most suitable method could be looked into by testing the methods on a hull without efficient high aspect-ratio appendages. To check whether trends on small nuances of speed differences are captured accurately, full VPP sweeps could also be conducted for interim models. It should be tested in future research if it might be necessary to test interim models as new base models and adapt the experienced conditions at the operation points, especially in regard to heel to limit extrapolation. Additionally, the flaw in the application of the actuator discs into the VPP derivative method should be found.

REFERENCES

[1] International Maritime Organization (IMO)/ Marine Environment Protection Committee. "2023 IMO STRATEGY ON REDUCTION OF GHG EMISSIONS FROM SHIPS: RESOLUTION MEPC.377(80) Annex 15." (7.7.2023). Accessed 18.12.2024, URL https://wwwcdn.imo.org/localresources/en/OurWork/Environment/Documents/annex/MEPC%2080/Annex%2015.pdf.

[2] European Parliament and the Council. "REGULATION (EU) 2023/1805 on the use of renewable and low-carbon fuels in maritime transport, and amending Directive 2009/16/EC: Reg. 2023/1805: FuelEU Maritime Regulation." (13.9./2023). Accessed 19.12.2024, URL https://eur-lex.europa.eu/eli/reg/2023/1805.

[3] "2023 IMO Strategy on Reduction of GHG Emissions from Ships." (2023). URL https://www.imo.org/en/OurWork/Environment/Pages/2023-IMO-Strategy-on-Reduction-of-GHG-Emissions-from-Ships.aspx.

[4] BalticExchange. "Wind Assisted Ship Propulsion." Accessed 19.12.2024, URL https://emissions.balticexchange.com/en/Wind.html.

[5] Khan, L., Macklin, J. J. R., Peck, B. C. D., Morton, O. and Souppez, J-B R. G. "A REVIEW OF WIND-ASSISTED SHIP PROPULSION FOR SUSTAINABLE COMMERCIAL SHIPPING: LATEST DEVELOPMENTS AND FUTURE STAKES." *Wind Propulsion 2021* (2021)DOI 10.3940/rina.win.2021.05.

[6] Chou, Todd, Kosmas, Vasileios, Acciaro, Michele and Renken, Katharina. "A comeback of wind power in shipping: An economic and operational review on thewind-assisted ship propulsion technology." *Sustainability (Switzerland)* Vol. 13 (2021): pp. 1–16. DOI 10.3390/su13041880.

[7] Petkovic, Miro, Zubcic, Marko, Krcum, Maja and Pavic, Ivan. "Wind Assisted Ship PropulsionTechnologies – Can they Help in Emissions Reduction?" *Naše more* Vol. 68 No. 2 (2021): pp. 102–109. DOI 10.17818/NM/2021/2.6.

[8] Faber, Jasper, Hanayama, Shinichi, Shuang, Zhang, Pereda, Paula, Comer, Bryan, Hauerhof, Elena, van der Loeff, Wendela Schim, Smith, Tristan, Zhang, Yan, Kosaka, Hiroyuko, Adachi, Masaki, Bonello, Jean-Marc, Galbraith, Connor, Gong, Ziheng, Hirata, Koichi, Hummels, David, Kleijn, Anne, Lee, David S., Liu, Yiming, Lucchesi, Andrea, Mao, Xiaoli, Muraoka, Eiichi, Osipova, Liudmila, Qian, Haoqi, Rutherford, Dan, de la Fuente, Santiago Suárez, Yuan, Haichao, Perico, Camilo Velandia, Libo, Wu, Sun, Deping, Yoo, Dong-Hoon and Xing, Hui. "Fourth IMO GHG Study 2020." (2021).

[9] Bureau Veritas. "Technology Report: Wind Propulsion." Accessed 18.12.2024, URL https://marine-offshore.bureauveritas.com/newsroom/wind-propulsion-report.

[10] "Applying Wind-Assisted Propulsion to ships: Energy Efficiency Retrofit Report 2024." Accessed 18.12.2024, URL https://www.lr.org/en/knowledge/research-reports/2024/applying-wind-assisted-propulsion-to-ships/.

[11] Laursen, R., Patel, H., Sofiadi, D., Zhu, R., Nelissen, D., van Seters, D. and Pang, E. "Potential of Wind-assisted Propulsion for Shipping: By ABS, CE Delft & ARCSILA." Accessed 18.12.2024, URL https://emsa.europa.eu/publications/item/5078-potential-of-wind-assisted-propulsion-for-shipping.html.

[12] Čalić, Ante, Jurić, Zdeslav and Kotalinić, Marko. "Impact of Wind-Assisted Propulsion on Fuel Savings and Propeller Efficiency: A Case Study." *Journal of Marine Science*

and Engineering Vol. 12 No. 11 (2024): p. 2100. DOI 10.3390/jmse12112100.

[13] Kolk, Nico Van Der. "Sailing Efficiency and Course Keeping Ability of Wind Assisted Ships." (2020)DOI 10.4233/uuid:8707309f-b9a3-4e09-916d-8fb64328a138. URL https://doi.org/10.4233/uuid:8707309f-b9a3-4e09-916d-8fb64328a138.

[14] Plessas, Timoleon and Papanikolaou, Apostolos. "Optimization of Ship Design for the Effect of Wind Propulsion." *International Marine Design Conference* (2024)DOI 10.59490/imdc.2024.884.

[15] Tillig, Fabian. "Simulation model of a ship´s energy performance and transportation costs." Dissertation, Chalmers tekniska högskola. 2020.

[16] Renzsch, Hannes and Thies, Fabian. "Hydrodynamic Optimization of Ships with Retrofitted WASP-Systems." Ecole Navale (ed.). *Innovsail*: pp. 363–380. 2023.

[17] Kramer, Jarle Vinje and Steen, Sverre. "Sail-induced resistance on a wind-powered cargo ship." *Ocean Engineering* Vol. 261 (2022): p. 111688. DOI 10.1016/j.oceaneng.2022.111688.

[18] Giovannetti, L. Marimon, Olsson, F., Alexandersson, M., Werner, S. and Finnsgård, C. "The Effects of Hydrodynamic Forces on Maneuvrability Coefficients for Wind-Assisted Ships." *Proceedings of the ASME 39th International Conference on Ocean, Offshore and Arctic Engineering - 2020*. 2020. The American Society of Mechanical Engineers, New York, N.Y. DOI 10.1115/OMAE2020-18673.

[19] Thies, Fabian and Renzsch, Hannes. "Hull Form Variations for Improved Sailing Balance of Wind-Assisted Propelled Ships." Bertram, Volker (ed.). *HIPER'24*: pp. 218–225. 2024.

[20] Bataille, Juliette, Blayo, Camille and Sergent, Pierrick. "PERFO: Methodology benchmark for Wind Assisted Propulsion Ship Performance Estimation." Ecole Navale (ed.). *Innovsail*: pp. 307–320. 2023.

[21] Tannenberg, Rafael, Turnock, Stephen R., Hochkirch, Karsten and Boyd, Stephen W. "VPP Driven Parametric Design of AC75 Hydrofoils." *Journal of Sailing Technology* Vol. 8 No. 01 (2023): pp. 161–182. DOI 10.5957/jst/2023.8.9.161.

[22] Kramer, Jarle, Steen, Sverre and Savio, Luca. "Drift Forces - Wingsails vs Flettner Rotors." 2016.

[23] Gerritsma, J, Keuning, J A and Versluis, A. "Sailing yacht performance in calm water and in waves." (1993).

[24] Munk, Max M. "Remarks on the Pressure Distribution over the Surface of an Ellipsoid Moving Translationally Through a Perfect Fluid." (1924).

[25] van der Kolk, Nico, Bordogna, Giovanni, Mason, J.C., Desprairies, P. and Vrijdag, Arthur. "Case Study: Wind-assisted ship propulsion performance prediction, routing, and economic modelling." 2019. Royal Institution of Naval Architects (RINA).

[26] Chica, Manuel, Hermann, Roberto Rivas and Lin, Ning. "Adopting different wind-assisted ship propulsion technologies as fleet retrofit: An agent-based modeling approach." *Technological Forecasting and Social Change* Vol. 192 (2023): p. 122559. DOI 10.1016/j.techfore.2023.122559.

[27] Ballini, Fabio, Ölçer, Aykut I., Brandt, Jørgen and Neumann, Daniel. "Health costs and economic impact of wind assisted ship propulsion." *Ocean Engineering* Vol. 146 (2017): pp. 477–485. DOI 10.1016/j.oceaneng.2017.09.014.

[28] Wei, Xinxin, Yan, Tianhong, Sun, Tao, Liu, Shulin and Du, Hongyi. "Research on the hydrodynamic performance of propellers under oblique flow conditions." *Proceedings of the Institution of Mechanical Engineers, Part M: Journal of Engineering for the Maritime Environment* Vol. 238 No. 4 (2024): pp. 728–737. DOI 10.1177/14750902241231349.

[29] Nouroozi, Hossein and Zeraatgar, Hamid. "Propeller Hydrodynamic Characteristics in Oblique Flow by Unsteady Ranse Solver." *Polish Maritime Research* Vol. 27 No. 1 (2020): pp. 6–17. DOI 10.2478/pomr-2020-0001.

[30] Alterskjaer, S. A., Eggers, R., Gao, Y., Kim, Y., Kume, K., Trodden, D., Werner, Sofia and Zhang, X. "ITTC - Recommended Procedures and Guidelines: Guideline: Predicting the Power Saving of Wind Powered Ships: 7.5-02-03-01.9." Accessed 3.12.2024, URL https://www.ittc.info/media/11806/75-02-03-019.pdf.

[31] Hillege, Wick. "On the potential of using non-stationary full-scale NMEA data strings to gain insight in the performance of a stationary velocity prediction program for sailing yachts." Master's Thesis, Delft University of Technology. 2021.

[32] Böhm, Christoph. "A Velocity Prediction Procedure for Sailing Yachts with a hydrodynamic model based on integrated fully coupled RANSE-Free-Surface simulations." (2014).

[33] *ORC VPP Documentation 2022* (2022).

[34] Reche-Vilanova, Martina, Hansen, Heikki and Bingham, Harry B. "Performance Prediction Program for Wind-Assisted Cargo Ships." *Journal of Sailing Technology* Vol. 6 No. 01 (2021): pp. 91–117. DOI 10.5957/jst/2021.6.1.91.

[35] Sparreboom, Daan. "Weather routing of motorsailers." (2012).

[36] van der Kolk, N. J., Keuning, J. A. and Huijsmans, R.H.M. "Part 1: Experimental validation of a RANS-CFD methodology for the hydrodynamics of wind-assisted ships operating at leeway angles." *Ocean Engineering* Vol. 178 (2019): pp. 375–387. DOI 10.1016/j.oceaneng.2018.12.041.

[37] van der Kolk, N. J., Akkerman, I., Keuning, J. A. and Huijsmans, R.H.M. "Part 2: Simulation methodology and numerical uncertainty for RANS-CFD for the hydrodynamics of wind-assisted ships operating at leeway angles." *Ocean Engineering* Vol. 201 (2020): p. 107024. DOI 10.1016/j.oceaneng.2020.107024.

[38] Nikkels, Thys. "The Ecoliner concept." (2013).

[39] Mobron, Emiel. "Improving the performance of a sail-assisted cargo vessel." Master's Thesis, Delft Univeristy of Technology. 2014.

[40] Watson, David G.M. *Practical Ship Design*. Vol. 1. Elsevier Ocean Engineering Book Series (1998).

[41] Parson, Michael G. *Parametric Design*. The Society of Naval Architects and Marine Engineers (2003): .
[42] "Blue Route (Marin)." URL https://blueroute.application.marin.nl.
[43] van der Kolk, N. J., Akkerman, I., Keuning, J. A. and Huijsmans, R. H. M. "Low-aspect ratio appendages for wind-assisted ships." *Journal of Marine Science and Technology* Vol. 26 (2021): pp. 1126–1143. DOI 10.1007/s00773-020-00777-8.

